Photo-Ionized Lithium Source for Plasma Accelerator Applications

P. Muggli, K. A. Marsh, S. Wang, C. E. Clayton, S. Lee, T. C. Katsouleas, and C. Joshi

***Abstract*— A photo-ionized lithium source is developed for plasma acceleration applications. A homogeneous column of lithium neutral vapor with a density of 2×10^{15} cm^{-3} is confined by helium gas in a heat-pipe oven. A UV laser pulse ionizes the vapor. In this device, the length of the neutral vapor and plasma column is 25 cm. The plasma density was measured by laser interferometry in the visible on the lithium neutrals and by CO_2 laser interferometry on the plasma electrons. The maximum measured plasma density was 2.9×10^{14} cm^{-3}, limited by the available UV fluence ($\approx$83 mJ/cm^2), corresponding to a 15% ionization fraction. After ionization, the plasma density decreases by a factor of two in about 12 μs. These results show that such a plasma source is scaleable to lengths of the order of 1 m and should satisfy all the requirements for demonstrating the acceleration of electrons by 1 GeV in a 1-GeV/m amplitude plasma wake.**

***Index Terms*— Alkali plasma, electron acceleration, heat-pipe oven, plasma accelerator, wakefield.**

I. Introduction

RECENT experimental results on electron acceleration in relativistic plasma waves demonstrate energy gains up to 100 MeV [1], [2]. The maximum energy observed in these experiments is limited by the length over which the large amplitude coherent plasma waves (wakes) can be excited or by phase slippage between the accelerated electrons and the wake. In the laser wakefield acceleration (LWFA) scheme [1], [3] accelerating gradients greater than 100 GeV/m have been excited over a distance of approximately 1 mm with a plasma density n_e in the 10^{19} cm^{-3} range. In the plasma beat-wave acceleration (PBWA) scheme [2], gradients of the order of 3 GeV/m are excited over 1 cm ($n_e \approx 10^{16}$ cm^{-3}). In all these experiments, the energy gain W can be estimated from a simple scaling law resulting from the product of the accelerating wake amplitude obtained from Poisson's equation times the accelerating length

$$W[\mathrm{MeV}] = 96\varepsilon L[\mathrm{cm}]\sqrt{n_e[\mathrm{cm}^{-3}]/10^{16}} \tag{1}$$

where $\varepsilon = \delta n_e/n_e$ is the wake amplitude ($\varepsilon \leq 1$, typically $0.3 < \varepsilon < 0.5$), and L is the shorter of the length over which the wake is excited or the dephasing length, i.e., the length in the laboratory frame in which the accelerating electrons slips by 90° in phase with respect to the plasma wave. Future experiments will aim at demonstrating energy gains of the order of 1 GeV. This can be achieved in an $n_e \approx 10^{18}$ cm^{-3} plasma with a length $L \approx 1$ cm, in an $n_e \approx 10^{16}$ cm^{-3} plasma with $L \approx 10$ cm, or in an $n_e \approx 10^{14}$ cm^{-3} plasma with a length $L \approx 1$ m. Although in the latter case the gradient is not as high as already achieved in other plasma-based acceleration experiments, the 1-GeV/m gradient is much larger than that achieved in any accelerating metallic structure.

Recently, a plasma-wakefield acceleration (PWFA) [4] experiment has been proposed at the final focus test beam (FFTB) of Stanford Linear Accelerator Center (SLAC) in which the goal is to demonstrate electron acceleration by 1 GeV in a 1-m long plasma [5]. In that experiment, known as E-157, the bulk of a 30-GeV SLAC-FFTB electron bunch drives a 1-GeV/m plasma wake, while the trailing electrons of the same bunch act as witness particles and experience the acceleration by the electric field of this wake. An energy gain of 1 GeV is, in principle, possible if a wake is excited over a distance of 1 m in an $n_e \approx 2$–4×10^{14} cm^{-3} plasma. The high energy of the driving/witness electron bunch makes it insensitive to instabilities and energy depletion over the length of the experiment. Over the 1 m, the accelerated particles will not significantly phase slip since the dephasing length for the $\approx$30 GeV electrons, defined as $L_d = \pi c\gamma_{\mathrm{ph}}^2/\omega_{\mathrm{pe}}$ (where γ_{ph} is the relativistic factor of the electrons driving the wake and ω_{pe} is the plasma frequency) is $\approx 4 \times 10^6$ m.

A prototype for a 1-m plasma source that should fulfill the requirements for the proposed experiment is described in this paper. In Section II, the plasma parameters required for the E-157 experiment are given. The heat-pipe oven in which the lithium vapor is produced is described in Section III. Temperature profile measurements taken along the oven axis are presented in Section IV. The results of three different methods used to measure the line-integrated lithium neutral density are compared in Section V. Section VI discusses plasma density measurement results obtained by interferometry at three different wavelengths and by UV laser light absorption. The implications for scaling this source to a 1-m long plasma

Manuscript received November 17, 1998. Supported by the U.S. Department of Energy under Grants DE-FG03-92ER40727 and DE-FG03-92ER40745, and by the National Science Foundation under Grants ECS-9632735 and ECS-9617089.

P. Muggli is with the Department of Electrical Engineering, University of California, Los Angeles, Los Angeles, CA 90095 USA and the Department of Electrical Engineering and Quantum Electronics, University of Southern California, Los Angeles, CA 90089 USA.

K. A. Marsh, S. Wang, C. E. Clayton, and C. Joshi are with the Department of Electrical Engineering, University of California, Los Angeles, Los Angeles, CA 90095 USA.

S. Lee and T. C. Katsouleas are with the Department of Electrical Engineering and Quantum Electronics, University of Southern California, Los Angeles, CA 90089 USA.

Publisher Item Identifier S 0093-3813(99)05501-0.

TABLE I
PARAMETERS FOR THE SLAC-FFTB DRIVING ELECTRON BEAM [5]

Number of Electrons	N_e	3.5-4.0 $\times$ 10^{10}
Initial Energy	E_0	30 GeV
Bunch Length	σ_z	0.6 mm
Bunch Size (@ 1 $\times$ 10^{10}e$^-$)	σ_x	23 μm
	σ_y	37 μm
Emittance	$\gamma_{\rm ph}\varepsilon_x$	60 mm-mrad
	$\gamma_{\rm ph}\varepsilon_y$	15mm-mrad

TABLE II
PLASMA PARAMETERS REQUIRED FOR THE E-157 EXPERIMENT [5]

Plasma Density	n_e	2$-$4 $\times$ 10^{14}cm^{-3}
Plasma Length	L	1 m
Density Uniformity	$\Delta n_e/n_e$	< 25%
Ionization Fraction	n_e/n_0	> 15%
Radius	r	> 400 μm

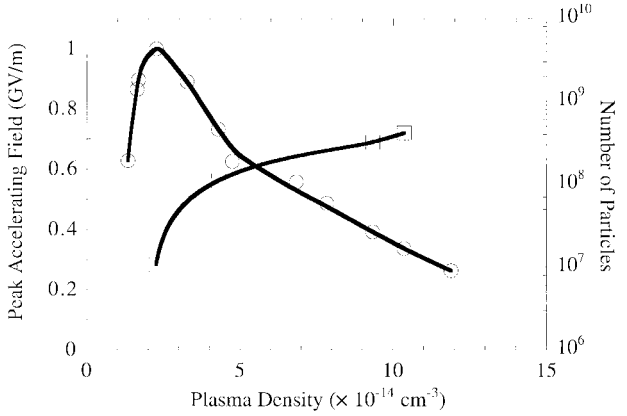

Fig. 1. Peak accelerating gradient (circles) and number of particles experiencing more than 70% of the gradient (squares) versus plasma density as obtained from PIC simulations for an electron bunch $\sigma_z = 0.6$ mm with $N = 4 \times 10^{10}$ electrons. The lines are added to guide the eye.

are briefly discussed in Section VII, and a summary and conclusions are given in Section VIII.

II. PLASMA REQUIREMENTS

The plasma parameters required for the E-157 experiments can be deduced for the SLAC-FFTB beam parameters (Table I) and from numerical particle in cell (PIC) computer simulations [5]. The deduced parameters are listed in Table II.

An electron plasma density n_e adjustable between 2 and 4 $\times$ 10^{14} cm^{-3} over 1 m is needed to optimize the energy gain and the number of accelerated particles. Fig. 1 shows that the maximum gradient (900$\pm$100 MeV/m) is reached with $n_e = 2.1 \times 10^{14}$ cm^{-3}. However, in the experiment, the plasma density may have to be increased in order to accelerate a number of particles sufficient for the detection system. Fig. 1 shows that, although the accelerating gradient monotonically decreases once the plasma density is increased beyond its optimum value of 2 $\times$ 10^{14} cm^{-3}, the number of accelerated particles increases with the plasma density as more and more electrons in the tail of that bunch are accelerated by the wakefield of shorter and shorter wavelength.

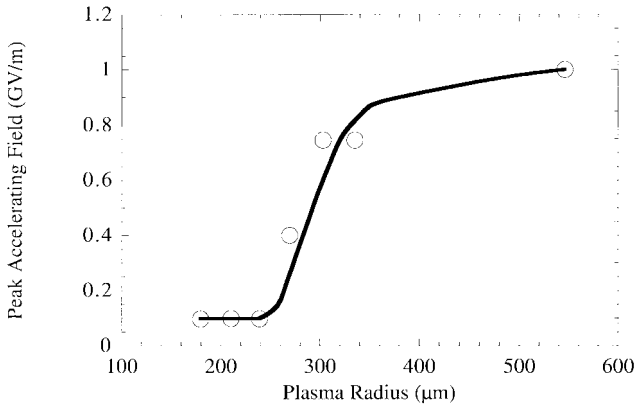

Fig. 2. Peak accelerating gradient as a function of the plasma radius as obtained from PIC simulations. For $r < 400$ μm, the electrons of the plasma are blown out of the plasma by the electron bunch. Parameters: $N = 4 \times 10^{10}$ electrons, $\sigma_z = 0.6$ mm, beam radius 75 μm, $n_0 = 2 \times 10^{14}$ cm^{-3}. The line is added to guide the eye.

A minimum plasma density variation $\Delta n_e/n_e$ over 1 m is required to avoid substantial dephasing between the accelerated particles and the plasma wake. A variation $\Delta n_e/n_e$ of 25% leads to a 12% variation in the wavelength of the plasma accelerating structure or 45° of phase slip for the accelerating electrons. For a linear gradient over the 1-m long plasma, the corresponding average reduction in the maximum energy gain is 15%.

A minimum plasma radius of 400 μm is needed to avoid the degradation of the wake amplitude caused by the excursion of the plasma electrons outside of the plasma when blown out by the electron bunch, as shown on Fig. 2.

An adjustable plasma length L and sharp plasma/neutral boundaries are desired in order to match the electron bunch betatron wavelength [6] to a submultiple of L. When the electron beam enters the plasma and expels all the plasma electrons (blowout regime), the resultant plasma ion column generates a focusing force on the beam electrons. The transverse spot size of the beam oscillates at the betatron frequency with a corresponding longitudinal wavelength $\lambda_b = 2\pi c(2\gamma_{\rm ph})^{1/2}/\omega_{\rm pe}$ ($\approx$80 cm with $n_e = 2 \times 10^{14}$ cm^{-3}). At each plasma density, the length of the plasma column (i.e., that of the neutral column) has to be adjusted to $2L/\lambda_b = m$ ($m = 2$ or 3 for $L \approx 1$ m, $n_e = 2 - 4 \times 10^{14}$cm^{-3}) for the electron beam to have the same divergence angle at the exit as at the entrance of the plasma.

A low atomic number Z for the gas/plasma nuclei and a large fractional ionization ($n_e/n_0 > 15\%$, n_0 is the neutral density) will minimize the influence of impact ionization of the neutrals by the driving electron bunch. The ionization cross section being proportional to the atom size, i.e., its atomic number Z, the lowest possible Z is desired. The additional plasma density due to impact ionization is proportional to the product of the neutral density and the electron beam density. The beam density varies inside the plasma column as the beam executes betatron oscillations. Estimates [7] show that with a beam of $N_e = 3 \times 10^{10}$ electrons, an additional ionization fraction of about 1.6% for $Z = 2$ (He), and 4.5% for $Z = 10$ (Ne), could be generated by this process in the partially ionized

TABLE III
LITHIUM PHYSICAL CHARACTERISTICS [14]

Li Atomic Number	3
Atomic Weight	6.94
Density (@ 25 ° C)	0.534
Thermal Conductivity	0.847 $W \cdot cm^{-1} \cdot K^{-1}$
Heat Capacity @ 25 °C	3.582 $J \cdot g^{-1} \cdot K^{-1}$
Melting Point	180.54 °C
Boiling Point @ 1 atm.	1342 °C
Fusion Enthalpy	432 J/g
Vaporization Enthalpy	19 J/g
Ionization Potential: Li^{I}	5.392 eV
Ionization Potential: Li^{II}	75.638 eV

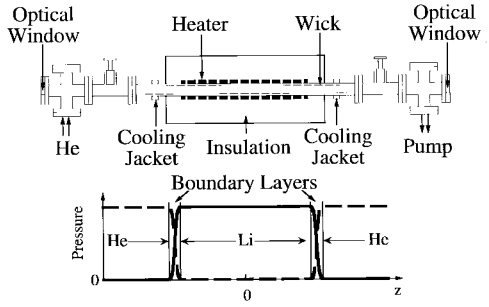

Fig. 3. Schematic of the heat-pipe oven (not to scale) and expected pressure profiles for the buffer gas (He) and the Li vapor (assuming no significant flow in the oven). The length of the Li column and width of the boundary layers are arbitrary on this figure.

plasma at the locations where the beam pinches to its minimum spotsize (≈0.5 μm). However, numerical simulations are under way to estimate the amount of ionization directly caused by the beam electrons and by the plasma electrons blown outside of the electron beam radius with kilovolts of kinetic energy.

Lithium (Li) is chosen (Table III) because it has the lowest ionization potential, and can thus be photo-ionized by UV light (1-photon process), and the lowest atomic number ($Z = 3$) simultaneously. The photo-ionized plasma is expected to have a very uniform transverse profile (over millimeters in radius with a smooth laser pulse profile), and a small longitudinal gradient ($\Delta n_e/n_e < 10\%$ over the 1 m) when double passed by the ionizing laser beam. Lithium vapor pressures corresponding to neutral densities in the 10^{15} cm^{-3} range—sufficient to satisfy the above-mentioned requirements—can be obtained in a heat-pipe oven at temperatures around 750 °C.

III. HEAT-PIPE OVEN

The heat-pipe oven, shown schematically in Fig. 3, consists of a stainless steel tube heated along its central part with water-cooled jackets at both ends and a stainless steel mesh "wick" encircling the inner wall of the tube [8]. The cold oven is filled with a given pressure P_{buffer} of helium buffer gas (≈200 mT in this experiment) and contains a 30-g ingot of Li. When heated, the Li melts and its vapor pressure increases. The Li vapor transports away from this evaporation zone and eventually condenses onto the wick some distance away. Condensation heats the wick through release of the Li heat of evaporation (19 J/g), while the transport of the vapor

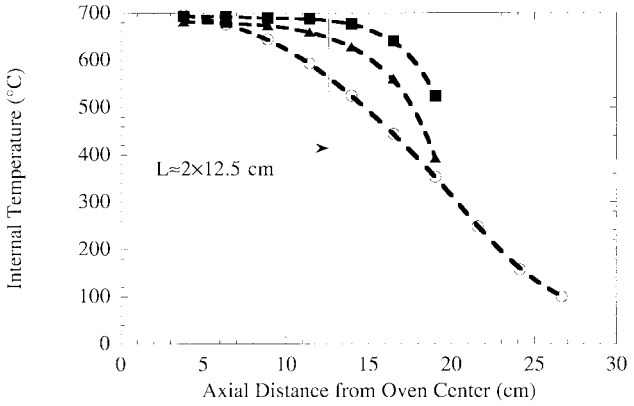

Fig. 4. Temperature profiles along the oven axis without Li in the oven and $P_{\text{heat}} = 250$ W (open circles) and with Li in the oven and $P_{\text{heat}} = 265$ W (filled triangles) and $P_{\text{heat}} = 307$ W (filled squares). The lines are drawn to guide the eye. The Li column length, defined as the length over which the density n_0 drops by 20% (according to the Li vapor pressure curve), is $L = 25$ cm with $P_{\text{heat}} = 307$ W and $T_{\text{ext}} = 750$ °C. $P_{\text{buffer}} = 200$ mT.

away from the center of the oven expels the helium buffer gas through lithium–helium collisions. As the heating power is increased, the evaporation rate of the liquid Li on the wick increases, as do the temperature and pressure of the Li vapor. At some heating power, the oven reaches a temperature such that the vapor pressure of the liquid Li is equal to P_{buffer}. The evaporation zone of the oven now contains a column of pure Li with $P_{\text{Li}} = P_{\text{buffer}}$ (assuming the Li flow velocity from the evaporation to the condensation zone of the oven is substantially subsonic). Collisional diffusion of the Li vapor at the helium boundary ensures that the Li condenses onto the wick (where it returns to the evaporation zone through capillary action) and does not penetrate more than a few collisional mean-free paths into the helium, thus forming sharp boundaries. Further increasing the heating power increases the evaporation rate but not the Li temperature. Instead, the column of Li vapor increases in length until the room-temperature boundary condition imposed by the water jackets ultimately limits the length of this column. The Li pressure and temperature (i.e., density n_0) are fixed by the buffer pressure, while the Li column length is proportional to the heating power.

The device described here has an inner diameter of 25.2 mm. It is heated over 40 cm, the insulation is 46 cm long, while the distance between the cooling jackets is 52 cm. Optical windows (quartz or BaF_2) are located at the ends of the oven and are in contact only with the room temperature buffer gas. They provide access for the ionizing laser pulse and for optical diagnostics of the Li vapor and the plasma.

IV. TEMPERATURE PROFILE MEASUREMENTS

The length over which the Li vapor extends is estimated from temperature profiles measured with a thermocouple probe inserted along the axis of the heat-pipe oven. The profile without Li in the oven (Fig. 4) shows that the temperature is decreasing away from the oven center due to heat conduction along the oven. In contrast, the profiles measured with Li in the oven and with comparable heating power exhibit a

relatively constant temperature in the center of the oven, followed by a rapid drop toward the end of the oven. The constant temperature in the central section of the heat-pipe oven is the result of the combination of the heat transport by the Li vapor and of the relatively high heat conductivity of the liquid Li on the wick. In this oven, the length over which the vapor density drops to 80% of the center density is estimated from the temperature profiles and the Li vapor pressure curve to be $L = 20$ cm with a heating power $P_{\text{heat}} = 265$ W, reaching an external wall temperature of $T_{\text{ext}} = 729\,^{\circ}\text{C}$, and $L = 25$ cm with $P_{\text{heat}} = 307$ W and $T_{\text{ext}} = 750\,^{\circ}\text{C}$. However, the temperature of the wick (and thus of the vapor) is expected to be more uniform than that measured by the thermocouple probe because of the heat conduction along the probe itself. Note that the temperature of the oven wall measured by a thermocouple placed outside of the oven, and referred to as T_{ext} hereafter, is about 60 °C higher than that measured inside the oven.

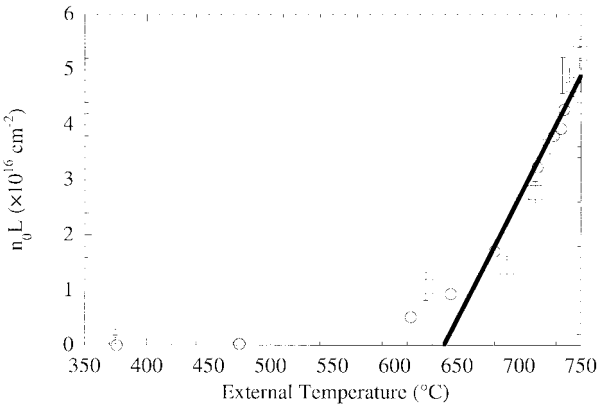

Fig. 5. Line-integrated neutral density n_0L as measured by the UV absorption method (squares) and by the hook method [11] (circles) with $P_{\text{buffer}} = 200$ mT. Assuming $L = 25$ cm at $T_{\text{ext}} = 750\,^{\circ}\text{C}$ (see Fig. 4), both methods show that $n_0 = 2 \times 10^{15}$ cm^{-3}. The line corresponds to a linear fit of n_0L as a function of T_{ext} for $T_{\text{ext}} > 640\,^{\circ}\text{C}$, yielding the Li column length L assuming $n_0 = 2 \times 10^{15}$ cm^{-3} in this range.

V. Neutral Density Measurements

In this section, three diagnostics for measuring the line-integrated Li neutral density n_0L are presented. With $L = 25$ cm when $T_{\text{ext}} = 750\,^{\circ}\text{C}$ (see Section IV), and assuming that the neutral Li density is fixed by the buffer gas pressure, i.e., that only L changes when $T_{\text{ext}} > 700\,^{\circ}\text{C}$, estimates for the average neutral density n_0 are obtained.

A. UV Absorption

A low energy (<100 μJ) laser pulse of 5.83 eV (UV) photons (frequency quintupled Nd:YAG, nanosecond laser pulse) is sent along the heat-pipe oven axis. It ionizes the Li vapor through a single-photon process (Li ionization potential: 5.392 eV). The line-integrated neutral density n_0L is obtained by measuring the ratio of the transmitted to incident UV energy

$$n_0L = -\frac{1}{\sigma}\ln\left(\frac{E_{\text{transmitted}}}{E_{\text{incident}}}\right) \tag{2}$$

where $\sigma = 1.8 \times 10^{-18}$ cm^{-2} is the ionization cross section for $h\nu = 5.83$ eV [9]. For this measurement, the incident and transmitted energies were monitored by photodiodes and their ratio calculated for each shot. Many shots were acquired at each oven external temperature and the ratios averaged. Fig. 5 shows the values of n_0L measured as a function of the oven external temperature. A value of 5.29×10^{16} cm^{-2} is obtained with $T_{\text{ext}} = 749\,^{\circ}\text{C}$, corresponding to $n_0 = 2.1 \times 10^{15}$ cm^{-3} for $L = 25$ cm. At this temperature (or neutral density), the fractional UV energy absorbed is only 9.5%.

B. White Light Absorption

Lithium, as do other alkali metals, exhibits a strong transition line in the visible frequency range from its ground state to the first excited state ($2s$ to $2p$ state, $J = 1/2 \rightarrow J' = 3/2$ at $\lambda = 670.78$ nm, and $J = 1/2 \rightarrow J' = 1/2$ at $\lambda = 670.79$ nm). However, for the experiments described here, the two Li transitions can be considered as one at $\lambda_{ij} = 670.785$ nm. Assuming that all of the Li atoms are in their ground state i, the electronic susceptibility χ_e at a frequency ω_0 associated with this $i \rightarrow j$ atomic transition is given by

$$\chi_e = \frac{N_i e^2}{\varepsilon_0 m_e}\sum_{j \neq i} f_{ij}\left(\omega_{ij}^2 - \omega_0^2 - i\omega_0/\tau_{ij}\right)^{-1} \tag{3}$$

where τ_{ij} is the natural lifetime of the upper state j, f_{ij} is the absorption oscillator strength of the transition, N_i is the population density of the lower level, and the sum runs over all the possible upper states j. In this case, only the transition at $\lambda_{ij} = 670.785$ nm needs to be considered for $\lambda \approx \lambda_{ij}$ since the closest other transition from the ground state is at $\lambda = 323.3$ nm ($2s \rightarrow 3p$). The relative dielectric constant ε_r is given by $\varepsilon_r = (1 + \chi_e)$. The corresponding dispersion is used to measure the neutral vapor density. Line-broadening effects can be included in (3) by replacing $1/\tau_{ij}$ by an effective line width $\Delta\omega$ that would include these effects. However, these effects are important only for the calculation of the imaginary part of χ_e or at frequencies very close to ω_{ij} (within a few line widths).

The imaginary part of χ_e is used to calculate the energy absorption coefficient γ

$$\gamma = -2k'' = \frac{-1}{k'}\frac{\omega_0^2}{c^2}\chi_e'' \tag{4}$$

where the prime ($'$) and double prime ($''$) stand for the real and imaginary part of the variable, and $k^2 = \varepsilon_r\omega_0^2/c^2$. Assuming $\omega_0 \approx \omega_{ij}$, and $\chi' \ll 1$, γ can be written as

$$\gamma(\omega) \cong \frac{-1}{2c}\frac{N_i e^2}{\varepsilon_0 m_e}\frac{f_{ij}\Delta\omega/2}{(\omega_{ij} - \omega)^2 + (\Delta\omega/2)^2}. \tag{5}$$

The sum in (3) has been dropped since the absorption of a single line is measured. Away from line center, the line shape is Lorentzian, and only the natural lifetime width and the self-broadening pressure term contribute to the effective line width $\Delta\omega$

$$\Delta\omega = \Delta\omega_{\text{natural}} + \delta\omega_s\frac{N_i}{N_0} \tag{6}$$

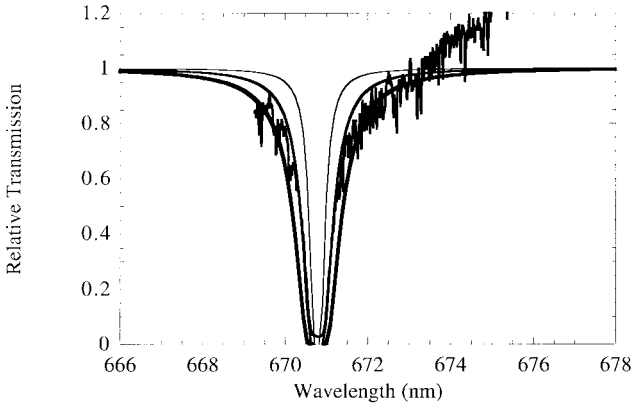

Fig. 6. White light spectrum around the $\lambda_{ij} = 670.785$ nm of Li, with $T_{\rm ext} = 750$ °C and $P_{\rm buffer} = 200$ mT. Also shown, the normalized absorption curves calculated from (5) and (6) with $n_0 = 2 \times 10^{15}$ cm^{-3} (thin line), $n_0 = 4 \times 10^{15}$ cm^{-3} (medium line), and $n_0 = 6 \times 10^{15}$ cm^{-3} (thick line).

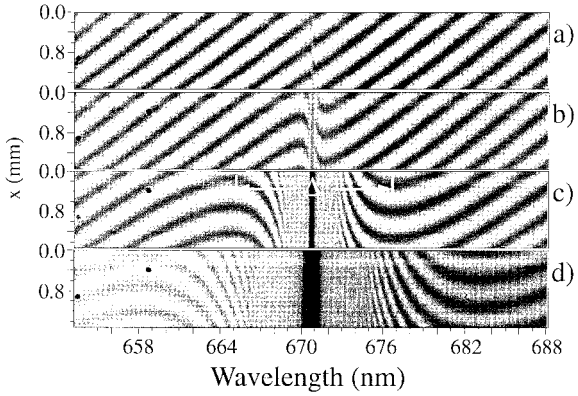

Fig. 7. Interferograms (hook method [11]), observed in the plane of the imaging spectrograph, showing the hooks created by the dispersion associated with the $2s \rightarrow 2p$ transition of the Li atom ($\lambda_{ij} = 670.785$ nm). (a) $T_{\rm ext} = 376\,^{\circ}$C, $\Delta_{ij} = 0.3$ nm, $n_0 L < 0.001 \times 10^{16}$ cm^{-2}, (b) $T_{\rm ext} = 475\,^{\circ}$C, $\Delta_{ij} = 1.8$ nm, $n_0 L = 0.024 \times 10^{16}$ cm^{-2}, (c) $T_{\rm ext} = 645\,^{\circ}$C, $\Delta_{ij} = 11.4$ nm (shown), $n_0 L = 0.93 \times 10^{16}$ cm^{-2}, and (d) $T_{\rm ext} = 737\,^{\circ}$C, $\Delta_{ij} = 24.4$ nm, $n_0 L = 4.7 \times 10^{16}$ cm^{-2}. In (d), $L \approx 23$ cm with $n_0 = 2 \times 10^{14}$ cm^{-3} (see Fig. 5). The vertical axis x is the distance along the imaging spectrometer slit representing a vertical cord through the oven. Only ≈1.4 mm is presented here.

where $\Delta\omega_{\rm natural} = 1/\tau_{ij}$, $\tau_{ij} = 26.9$ ns, and $\delta\omega_s = 36.8$ cm^{-1} [10] for the $2p$ level of Li, and $N_0 = 2.69 \times 10^{19}$ cm^{-3} is the number of atoms in 1 cm^{-3} of gas at room temperature and 1 atm.

A white light beam is sent along the axis of the oven and dispersed is a spectrograph to observe the absorption ($\approx e^{\gamma(\lambda)L}$) as a function of λ around $\lambda_{ij} = 670.785$ nm. Using (5) and (6), the absorption curve can be fitted to the measured data to deduce $n_0 = N_i$ assuming a given length L. Fig. 6 shows that with $T_{\rm ext} = 750\,^{\circ}$C, and assuming $L = 25$ cm, the experimental absorption curve is bracketed by the $n_0 = 4 \times 10^{15}$ cm^{-3} and the $n_0 = 6 \times 10^{15}$ cm^{-3} curves. Note that the absorption at line center is not used because it would require a precise measurement of the light transmission ($<10^{-6}$) within the absorption line width. The numerical fit is thus applied to the Lorentzian wings of the absorption curve. This method seems to overestimate the value of n_0 when compared to the results obtained using other methods (Paragraph A and C). The value of n_0 depends critically on the estimate of the line width [$\Delta\omega$ appearing in the numerator of (5)], a quantity not measured in this experiment. Methods that rely only on the real part of the relative dielectric constant of the Li vapor or plasma (independent of $\Delta\omega$ away from line center) are therefore used from now on.

C. Hook Method

The oven is placed in one arm of a Mach–Zehnder white light interferometer. The interferometer light is sent to a stigmatic, f/4, 27-cm spectrograph to observe the dispersion ($n(\lambda_0) = [\varepsilon_r(\lambda_0)]^{1/2}$, see Section V-B) in the vicinity of the neutral Li line at 670.785 nm (hook method [11]) as shown on Fig. 7. The line-integrated neutral density is obtained from the hook interferograms using the following formula:

$$n_0 L = N_i L \frac{\pi K}{r_0 \lambda_{ij}^3 f_{ij}} \Delta_{ij}^2 \tag{7}$$

where N_i is the population of the lower level i, K is the hook-interferogram constant [11], $r_0 = 2.82 \times 10^{-15}$ m is the classical electron radius, and Δ_{ij} is the hook separation of the $i \rightarrow j$ transition (see Fig. 7). Note that $n_0 L$ does not depend on the linewidth $\Delta\omega$. The transition originates from the ground state of the Li atom with $f_{ij} = 0.75$. The thermal energy of the Li atoms is low ($k_B T_{\rm Li} \leq h\nu_{ij}$), and the population of the ground state is therefore a very good approximation for the vapor density ($n_0 = N_i$). The measured values of $n_0 L$ obtained by this method are shown in Fig. 5 as a function of the oven external temperature. A value of 4.27×10^{16} cm^{-2} is obtained with $T_{\rm ext} = 736\,^{\circ}$C. In Fig. 7, the vertical axis corresponds to the distance along a vertical cord in the heat-pipe oven. The actual interferograms cover a distance of ≈6.8 mm and exhibit no variation of Δ_{ij} over that length, indicating a constant transverse profile of $n_0 L$ over at least that distance. The values of $n_0 L$ obtained by the hook method are in very good agreement with the value obtained by the UV absorption method; see Fig. 5.

The buffer gas pressure for all the measurements presented here is 200 mT. Assuming that the Li vapor is an ideal gas, and assuming that the Li flow in the oven is slow as compared to the sonic speed, n_0 would be 2.0×10^{15} cm^{-3} at 963 K of internal temperature ($T_{\rm ext} = 750\,^{\circ}$C). This density value agrees very well with the values of n_0 obtained assuming $L = 25$ cm. For the following measurements, ($T_{\rm ext} > 700\,^{\circ}$C), the column length can be deduced from Fig. 5 with the density assumed to be constant at $n_0 = 2 \times 10^{15}$ cm^{-3}. For the case of Fig. 7(d) ($T_{\rm ext} = 737\,^{\circ}$C), $n_0 L = 4.27 \times 10^{16}$ cm^{-2} corresponds to $L = 23.4$ cm, in excellent agreement with the length estimated from the temperature profile measurements described here above.

VI. Lithium Plasma

Changes in the neutral and/or plasma density modify the dielectric constant of the Li vapor and are measured by interferometry. The relative dielectric constant ε_r at frequency ω_0 near an atomic transition at frequency ω_{ij} of a partially

ionized gas is given by

$$\varepsilon_r = 1+\chi_e+\chi_{\rm pe} \cong 1+\frac{N_i e^2}{\varepsilon_0 m_e}\sum_{j\neq i}\frac{f_{ij}}{(\omega_{ij}^2-\omega_0^2)}-\frac{\omega_{\rm pe}^2}{\omega_0^2} \quad (8)$$

where χ_e is the neutral gas susceptibility, $\chi_{\rm pe}$ the plasma electron susceptibility, and $\omega_{\rm pe}^2 = n_e e^2/\varepsilon_0 m_e$ is the electron plasma frequency squared. It includes a contribution from the resonant transitions (change in N_i) from the lower state i of the neutral atoms to the possible upper states j of the transition (see Section V-C) and a contribution from the electron plasma density n_e. Upon ionization, the plasma density n_e is created, whereas a fraction ΔN_i of the neutral population density N_i disappears. Depending on ω_0, one or both of the contributions need to be retained. The change in index of refraction in one arm of the interferometer arising from the change in ε_r creates a phase difference $\Delta\Phi$ between the two arms and is given by

$$\Delta\Phi = 2\pi(n-1)\frac{L}{\lambda_0} \quad (9)$$

where $n = (\varepsilon_r)^{1/2}$. Interferometry can resolve density evolution during both the ionization and plasma disappearance (by recombination and/or diffusion) when these processes are slow. In the case of laser-ionized plasmas, the ionization process is often too fast (a few nanoseconds) to be resolved in time. Only the "unwinding" of the fringes resulting from plasma recombination or diffusion (or a combination of both) can be observed. However, when the interferometer wavelength and the maximum plasma density are such that the phase shift $\Delta\Phi$ is smaller than π (fraction of a fringe), the maximum n_e can be measured from the step in the interferometer trace corresponding to the unresolved, "instantaneous" ionization.

In this experiment, the plasma is created by ionizing the Li vapor with a 20-ns UV light pulse of an ArF excimer laser at 193 nm ($h\nu_{\rm uv} = 6.43$ eV) with a rectangular spot shape of area $A = 1.0\times 0.67$ cm^2. The length of the Li plasma is equal to the length L of the Li vapor.

A. CO_2 Laser Interferometry and UV Absorption

The line-integrated plasma density $n_e L$ is directly measured by CO_2 laser interferometry ($\lambda_0 = 10.6$ μm). At this wavelength, only the plasma electron contribution to ε_r needs to be retained. The relative contributions of the neutrals and the plasma to ε_r are about 1 : 355 and have the same sign. The plasma source is placed in one arm of a Mach–Zehnder interferometer. The product $n_e L$ is obtained by measuring the phase shift of the interferometer signal resulting from the change in index of refraction of the recombining plasma

$$n_e L \cong -\frac{\Delta\Phi}{\pi}\lambda_0 n_{\rm crit} \quad \text{for } n_e \ll n_{\rm crit} \quad (10)$$

where $n_{\rm crit} = (2\pi c/\lambda_0)^2\varepsilon_0 m_e/e^2 = 9.9\times 10^{18}$ cm^{-3} is the critical plasma density for λ_0. A $\Delta\Phi = \pi$ corresponds to $n_e L = 1.0\times 10^{16}$ cm^{-2}. Fig. 8 shows the plasma density measured by CO_2 interferometry with $T_{\rm ext} = 720\,^\circ$C and $L = 19$ cm, as a function of the UV fluence incident upon the Li vapor. The maximum density of $\approx 1.5\times 10^{14}$ cm^{-3} is limited by the UV energy reaching the Li vapor. The CO_2 laser pulse was coupled into the oven by grazing reflection ($\approx 70^\circ$) from a quartz window. When traversing this window, about half of the ionizing laser pulse energy was lost by reflection. The fractional ionization was about 7.5% in this case. The time for the plasma to drop by a factor of two, because of recombination and possible diffusion, is about 12 μs.

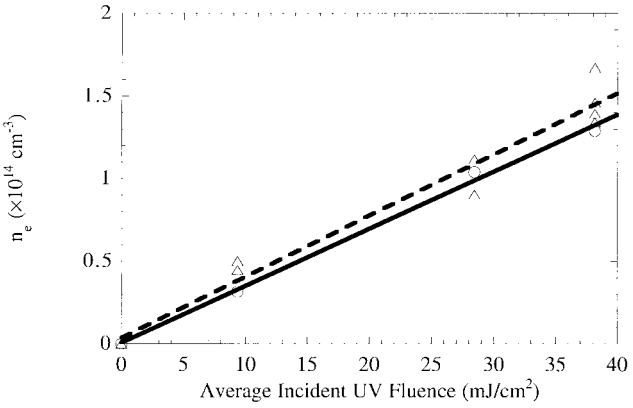

Fig. 8. Plasma density as measured by CO_2 interferometry (triangles, dashes line), and by absorption of the UV ionizing laser pulse energy (circles, continuous line) as a function of the UV fluence incident upon the Li vapor. The neutral density n_0 is 2.0×10^{15} cm^{-3}, $L = 19$ cm, and the UV absorption is 6.6%.

The average plasma density n_e is also estimated from the absorbed UV energy and from the illuminated volume since every photon absorbed by an atom creates one free electron. About 6.6% of the UV energy is absorbed over the 0.67 cm^2 beam cross-sectional area A and length $L = 19$ cm. The average plasma density calculated by this method is also plotted on Fig. 8 and shows a good agreement with the interferometry results. For a given initial neutral density n_0, the plasma density is expected to vary linearly with the incident UV energy

$$n_e \cong \frac{1}{AL}\frac{E_{\rm uv}}{h\nu_{\rm uv}}(1-\sigma n_0 L) \quad (11)$$

for $\sigma n_0 L \ll 1$. Note that for this measurement, the UV energies are averaged over a large number of laser pulses by a calorimeter. Shot-to-shot variation of the UV energy ($\pm 10\%$) is responsible for the variations in the plasma density observed by interferometry.

B. Helium-Neon Interferometry at $\lambda_0 = 633$ nm and CO_2 Laser Interferometry

Since the plasma is obtained by ionization of the neutrals, the plasma density can be inferred from the variation of the neutral Li density (change in N_i), i.e., by interferometry on the Li neutrals near $\lambda_{ij} = 670.785$ nm (see Section V-C). The wavelength at which interferometry is performed can be chosen to observe a suitable number of fringes. At $\lambda_0 = 10.6$ μm, only the plasma electron contribution to ε_r needs to be retained, whereas at $\lambda_0 = 633$ nm, the wavelength of the red helium–neon laser, both the neutrals and the plasma electron contribute to ε_r. The relative respective contributions to $\Delta\phi$ are about 6 : 1 assuming that $\Delta N_i = n_e$. Note that at

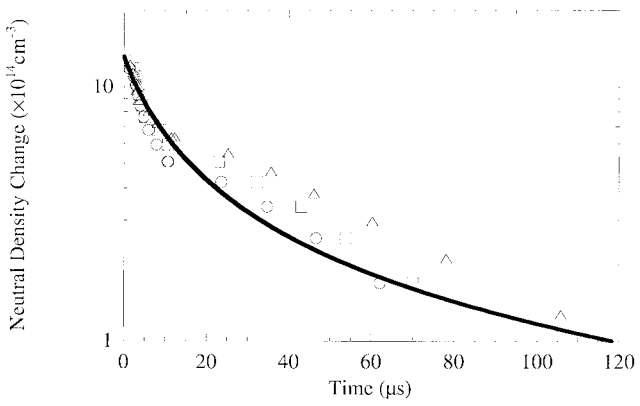

Fig. 9. Evolution of the neutral density ΔN_i for three shots at the same n_0, and with similar UV energies, as measured by interferometry at 674 nm. The inset show the oscillograms acquired for a single shot with two time scales: (a) 50 μs/division and (b) 2 μs/division. In both cases, the 20-ns laser pulse ionizes at the first division ($t = 0$). The time evolution is obtained by plotting the times at which the interferometric trace reaches an extremum ($\Delta\phi = \pi$). The laser pulse ionizes the Li vapor at $t = 0$. The line is the least square fit of the recombination equation solution [(13)] to the three sets of data and yields $n_{e0} = 12.2 \times 10^{14}$ cm^{-3} and $\alpha = 610 \times 10^{14}$ cm^3/s.

this wavelength the neutral contribution has a sign opposite to the plasma contribution. The average plasma density obtained at these two wavelengths are 1.2 $\times$ 10^{15} cm^{-3} and 4.0 $\times$ 10^{14} cm^{-3}, respectively, for a neutral density of 2.0 $\times$ 10^{15} cm^{-3} over $L = 9$ cm ($T_{\text{ext}} = 690\,^{\circ}$C) and an incident UV fluence of 30 mJ/cm^2. The value of n_e obtained from the UV absorption (3.1%) is 1.1 $\times$ 10^{14} cm^{-3} and is in good agreement with the CO_2 interferometry value. Note that the UV pulse spot shape is not uniform and may account for the discrepancy between the interferometry results. The UV absorption and the CO_2 interferometry yield volume-integrated values of the plasma density, whereas the helium–neon pencil beam only samples a cord along the oven axis. Interferometry on the Li neutrals at the helium–neon laser wavelength is a simple on-line diagnostic for n_e, suitable for a much longer plasma source such as the one that will be used in the actual acceleration experiment ($n_e \approx$ 2–4 $\times$ 10^{14} cm^{-3}). The plasma density measurement can be calibrated against the UV absorption and/or the CO_2 measurement.

C. Visible Interferometry at $\lambda_0 = 674$ nm

The interferometric trace at $\lambda_0 = 633$ nm showed only a phase shift of a fraction of a fringe ($\Delta\phi \approx \pi/10$), making it difficult to quantitatively reconstruct the unwinding of the fringe. However, a larger number of fringes are observed at a wavelength λ_0 closer to λ_{ij}. Fig. 9 show the time evolution of the Li neutral density after ionization as measured by interferometry at $\lambda_0 = 674$ nm using a diode laser. At this wavelength, the relative respective contributions to $\Delta\phi$ are about 78 : 1 (assuming that $\Delta N_i = n_e$) and have the same sign. Each $\Delta\phi = \pi$ corresponds to a plasma density of 0.82 $\times$ 10^{14} cm^{-3} (according to (8) and (9), $L = 23$ cm). The maximum density deduced from Fig. 9 is $n_e \approx 1.3 \times 10^{15}$ cm^{-3}. However, the heat-pipe temperature is $T_{\text{ext}} = 734\,^{\circ}$C ($n_0 \cong 2.0 \times 10^{15}$ cm^{-3} over $L = 23$ cm, Fig. 5) and the UV fluence 83 mJ/cm^2, leading to an average plasma density of 2.9 $\times$ 10^{14} cm^{-3}, and a fractional ionization n_e/n_0 of 14.5%, according to the UV absorption measurement.

The expression (8) for ε_r assumes that all the atoms are in their ground state ($N_j = 0$), and that only one resonant transition contributed to ε_r. These assumptions are well suited for the Li vapor prior to ionization: the thermal energy of the Li atoms is low ($k_B T_{\text{Li}} \ll h\nu_{ij}$), and the other possible transitions from the ground state are at wavelengths shorter than 324 nm. After ionization, however, the electrons recombine with the ions and populate all the levels of the Li atoms according to their respective recombination cross sections and according to the evolution to the electron temperature. The electrons are born with an excess energy of 1 eV. They thermalize with the neutrals and recombine with the ions. For low electron energies, calculated cross sections [12] show that np states have the largest recombination cross section. The recombination rate to the ground state is negligible compared to that of the upper states. The population of all the relevant levels and the transitions to and from them contribute to ε_r. In particular, the $2p$ state (the upper level for the 670.785-nm transition) can be populated either by direct recombination or by transitions from upper states. That would require the inclusion of a fourth term of the form $(N_j e^2/\varepsilon_0 m_e) f_{ji}(\omega_{ij}^2 - \omega_0^2)^{-1}$ in (8) where $f_{ji} = -(g_i/g_j) f_{ij}$, and $g_{i,j}$ is the statistical weight of the $i(j)$ state. This term has a sign opposite to that of the second term on the right-hand side of (8). Populating the upper state of the 670.785-nm transition would reduce ε_r and lead to an overestimation of the change in n_e ($n_e \neq \Delta N_i$). The time evolution of the population of the levels can, in principle, be described in a detailed analysis of these processes (rewriting (8) with a double sum on the i and j indexes). This is beyond the scope of this paper. Note that these atomic processes should affect only the interferometry at 674 nm, in which the interference fringes observed correspond to the plasma disappearance. The 633-nm interferometry relies on fringe shift corresponding to the "instantaneous" creation of the plasma, and so its interpretation is not complicated by the atomic physics in the "afterglow".

The plasma disappears from the probed volume because of recombination and/or ambipolar diffusion (Debye length $\lambda_d \approx 0.5$ μm for $T_e = 1$ eV and $n_e = 2 \times 10^{14}$ cm^{-3}). Plasma diffusion would lead to an exponential decay of n_e with time. Therefore, assuming that recombination is the dominant process as suggested by Fig. 9 (nonexponential decay for n_e), the time evolution of n_e is given by

$$\frac{\partial n_e}{\partial t} = \frac{\partial n_i}{\partial t} = -\alpha n_e n_i = -\alpha n_e^2 \tag{12}$$

where α is the recombination rate in cm^3/s. The solution to this recombination equation is

$$\frac{1}{n_e(t)} = \frac{1}{n_{e0}} + \alpha t \tag{13}$$

where n_{e0} is the initial electron density. A least square fit of this solution to the data of Fig. 9 leads to $\alpha = 610 \times 10^{14}$ cm^3/s. In this experiment, the electrons are born with an excess energy of 1 eV. The value of α calculated for Li assuming an initial Maxwellian distribution function for the free electrons

with a temperature $T_e = 10'000$ K is 25.8 $\times$ 10^{14} cm^3/s [12]. However, the electrons rapidly thermalize with the ions and neutral at $\approx$1000 K. The calculated values for α at this temperature is $\approx$150 $\times$ 10^{14} cm^3/s, which brings the measured values in good agreement with the calculated one. Estimation of the coefficients relevant for ambipolar diffusion yields a typical diffusion time of $\approx$1 ms.

Neutral Li has no metastable level, and the natural lifetimes of its excited state are shorter than a few hundreds of nanoseconds [12]. It is thus reasonable to assume that the relative time evolution of the plasma density inferred from Fig. 9, if not its absolute value, is governed by the recombination dynamics and not by the cascade decay once the electron has recombined with the ion.

The plasma density decreases by a factor of two in about 12 μs. This value is confirmed by CO_2 interferometry traces. This relatively slow time scale allows for the tuning of the plasma density in a wakefield experiment, such as the E-157, on a shot-to-shot basis by varying the delay between the laser ionizing pulse and the electron beam.

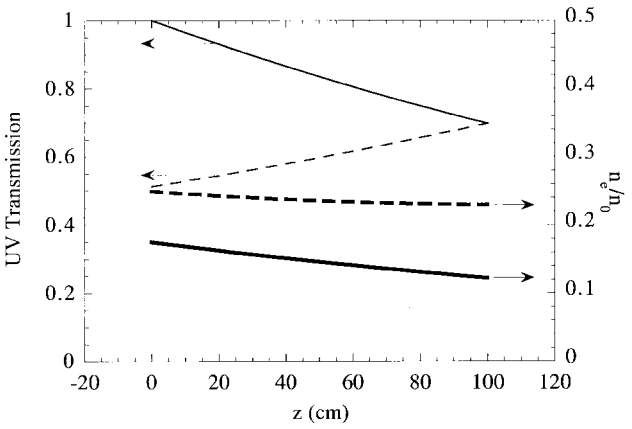

Fig. 10. Calculated transmission of the ionizing UV fluence (thin lines) and resulting fractional ionization n_e/n_0 (thick lines) along the 1-m long oven for the single pass case (solid lines) and the double pass case (dashed lines). In this example ($n_0 = 2 \times 10^{15}$ cm^{-3} and 100 mJ/cm^2), the average n_e is 3.0 $\times$ 10^{14} cm^{-3} ($n_e/n_0 = 15\%$) and $\Delta n_e/n_e = 36\%$ for a single pass, and the average n_e is 4.8 $\times$ 10^{14} cm^{-3} ($n_e/n_0 = 24\%$) and $\Delta n_e/n_e = 8\%$ for a double pass. Note that in the single- and double-pass case, the density gradient is negative along the single-pass laser beam path.

VII. Scaling to a 1-M Long Plasma Source

In scaling the 25-mm diameter, 25-cm long device described here to longer lengths, the concern is a possible pressure drop from the central section of the oven to its edges due to the finite flow velocity of the Li vapor. The Li vapor density profile would be nonhomogeneous and would not be fixed by the buffer gas pressure [13]. The conductance of the 1-m long oven is increased by going to an inner diameter of 38 mm. As in the case of the prototype device, the heater covers most of the oven length to minimize the length of the condensation zone of the oven and ensure a uniform longitudinal temperature profile. A heat shield is added between the heater and the thermal insulation to minimize the radial radiative losses, which dominate over conduction losses at high temperature. The thermal losses at the ends of the heat pipe will play a lesser role in the longer oven since the heated region is much longer than the typical distance over which the temperature is observed to drop with the prototype ($\approx$10 cm, see Fig. 4). A uniform vapor density is, of course, a prerequisite condition to obtain a uniform plasma density.

The average plasma density is proportional to the number of absorbed photons, which is proportional to the incident UV or photon fluence $N_{\rm uv}/A = E_{\rm uv}/h\nu_{\rm uv}A$ [(11)] and to n_0: $n_e = (n_0\sigma)\cdot(N_{\rm uv}/A)$. The fractional ionization is given by $n_e/n_0 = \sigma N_{\rm uv}/A$, and the plasma density gradient by $|\Delta n_e/n_e| = (\sigma n_0)^2\cdot(N_{\rm uv}/A)$. These expressions show that in order to maximize the plasma density and the fractional ionization, while minimizing the plasma density gradient, $N_{\rm uv}/A$ ($\propto$ UV energy fluence) rather than n_0 has to be increased.

At a given Li density, the total UV absorption is about four times larger in the 1-m long heat pipe than in the 25-cm prototype. The density variation from one end to the other of the heat pipe also increases in the same proportion. The density variation can be significantly reduced, from $\Delta n_e/n_e =$ 30% to 8% with $n_0 = 2 \times 10^{15}$ cm^{-3} with 100 mJ/cm^2, see Fig. 10, by double passing the UV ionizing laser pulse through the heat pipe. With the double-pass configuration and a given incident fluence, the average plasma density is also significantly increased (from $n_e = 3.0 \times 10^{14}$ cm^{-3} to 4.8 $\times$ 10^{14} cm^{-3}). A slight focusing of the UV laser pulse with a cylindrical lens can keep $N_{\rm uv}/A$ constant by compensating for photon absorption along the oven axis and thus offers an alternative to double passing the UV beam for maintaining a uniform density profile. In the above calculations, the neutral density is assumed to be uniform over the entire length of the heat pipe.

VIII. Summary and Conclusions

A lithium plasma source suitable for beam-driven plasma wakefield experiments is developed. A lithium vapor column with a density in the 2 $\times$ 10^{15} cm^{-3} range is obtained in a heat-pipe oven. The maximum length of the neutral Li column is about 25 cm. The values for the vapor density and column length obtained by the UV absorption and the hook method are in very good agreement. The white light absorption method overestimates n_0L. The vapor is ionized by 6.43 eV UV photons through a 1-photon process. The line-integrated plasma density is measured by CO_2 laser interferometry on the plasma electrons, by visible interferometry on the Li neutrals (near the $\lambda_{ij} = 670.785$ nm transition from the Li ground state), and by UV absorption. An excellent agreement is found between the UV absorption and the CO_2 interferometry results. The maximum plasma density is 2.9 $\times$ 10^{14} cm^{-3}, limited only by the maximum UV fluence available (83 mJ/cm^2). The time for the plasma density to drop by a factor of two is about 12 μs. Visible interferometry on the neutrals (helium-neon laser, $\lambda_{ij} = 633$ nm) provides a simple diagnostic for n_e and will be implemented in the SLAC E-157 experiment.

The present device has reached parameters desired in the 1-m long oven (n_0, n_e, and n_e/n_0). The results obtained with this plasma source device extrapolated to the 1-m long source

show that the source should satisfy the requirements (Table II) for the E-157 experiment. A 1-m source $(2L/\lambda_b \approx 3)$ is being built in collaboration with the Berkeley National Laboratory, and a 1.5-m $(2L/\lambda_b \approx 5)$ source is developed at UCLA for further experiments.

ACKNOWLEDGMENT

The authors would like to thank Prof. P. Muntz and Prof. D. Erwin from the University of Southern California for lending the excimer laser.

REFERENCES

[1] D. Gordon, K. C. Tzeng, C. E. Clayton, A. E. Dangor, V. Malka, K. A. Marsh, A. Modena, W. B. Mori, P. Muggli, Z. Najmudin, D. Neely, C. Danson, and C. Joshi, "Observation of electron energies beyond the linear dephasing limit from a laser-excited relativistic plasma wave," *Phys. Rev.*, vol. 80, no. 10, p. 2133, 1998.

[2] C. E. Clayton, K. A. Marsh, A. Dyson, M. Everett, A. Lal, W. P. Leemans, R. Williams, and C. Joshi, "Ultrahigh-gradient acceleration of injected electrons by laser-excited relativistic electron plasma wave," *Phys. Rev. Lett.*, vol. 70, no. 1, p. 37, 1993.

[3] T. Tajima and J. M. Dawson, "Laser electron accelerator," *Phys. Rev. Lett.*, vol. 43, no. 4, p. 705, 1979.

[4] P. Chen, J. M. Dawson, R. W. Huff, and T. C. Katsouleas, "Acceleration of electrons by the interaction of a bunched electron beam with a plasma," *Phys. Rev. Lett.*, vol. 54, no. 7, p. 693, 1985.

[5] T. Katsouleas, S. Lee, S. Chattopadhyay, W. L. Leemans, R. Assmann, P. Chen, F. J. Decker, R. Iverson, T. Kotseroglou, P. Raimondi, T. Raubenheimer, S. Ronki, R. H. Siemann, D. Walz, D. Whittum, C. E. Clayton, C. Joshi, K. Marsh, W. B. Mori, and G. Wang, "A proposal for a 1 GeV plasma-wakefield acceleration at SLAC," in *Proc. Particle Accelerator Conf.*, Vancouver, Canada, May 1997, pp. 1–4.

[6] T. C. Katsouleas, "Physical mechanisms in the plasma wakefield accelerator," *Phys. Rev. A*, vol. 33, no. 3, p. 2056, 1986.

[7] D. Gordon, C. E. Clayton, and C. Joshi, "Collisional ionization of gases by GeV beams," presented at the 7th Advanced Accelerator Concept Workshop, Lake Tahoe CA, 1996.

[8] C. R. Vidal and J. Cooper, "Heat-pipe oven: A new, well-defined metal vapor device for spectroscopic measurements," *J. Appl. Phys.*, vol. 40, no. 8, p. 3370, 1969.

[9] G. V. Marr, *Photoionization Process in Gases*. New York: Academic, 1967.

[10] W. W. Houston, "Resonance broadening of spectral lines," *Phys. Rev.*, vol. 54, p. 884, 1938.

[11] W. C. Marlow, "Hakenmethode," *Appl. Opt.*, vol. 6, no. 10, p. 1715, 1967.

[12] J. Lahiri and S. T. Manson, "Radiative recombination and excited-state photoionization of lithium," *Phys. Rev. A*, vol. 48, no. 5, p. 3674, 1993.

[13] C. R. Vidal, "Spectroscopic observation of subsonic and sonic vapor flow inside an open-ended heat pipe," *J. Appl. Phys.*, vol. 44, no. 5, p. 2226, 1973.

[14] *CRC Handbook of Chemistry and Physics*, 72nd ed. Boca Raton, FL: CRC Press 1991.

P. Muggli, photograph and biography not available at the time of publication.

K. A. Marsh, photograph and biography not available at the time of publication.

S. Wang, photograph and biography not available at the time of publication.

C. E. Clayton, photograph and biography not available at the time of publication.

S. Lee, photograph and biography not available at the time of publication.

T. C. Katsouleas, photograph and biography not available at the time of publication.

C. Joshi, photograph and biography not available at the time of publication.